

# Monthly Climatology of the Southern Ocean under Sea Ice

Kaihe Yamazaki<sup>1</sup>, Helen Elizabeth Phillips<sup>2</sup>, Maxim Nikurashin<sup>2</sup>, Laura Herraiz-Borreguero<sup>3</sup>, Paul Spence<sup>1</sup>, and Nathaniel L. Bindoff<sup>2</sup>

<sup>1</sup>Institute for Marine and Antarctic Studies, University of Tasmania

<sup>2</sup>University of Tasmania

<sup>3</sup>Commonwealth Scientific and Industrial Research Organisation

December 18, 2023

## Abstract

The advent of under-ice profiling float and biologging techniques has enabled year-round observation of the Southern Ocean and its Antarctic margin. These under-ice data are often overlooked in widely used oceanographic datasets, despite their importance in understanding the seasonality and its role in sea ice changes, bottom water formation, and glacial melt. We develop a four-dimensional climatology of the Southern Ocean (south of 40°S and above 2,000 m) using Data Interpolating Variational Analysis, which excels in multi-dimensional interpolation and consistent handling of topography and advection. The climatology captures thermohaline variability under sea ice, previously hard to obtain, and outperforms other products in data fidelity with smaller root-mean-square errors and biases. Our dataset will be instrumental for investigating seasonality and for improving ocean models. This work further highlights the quantitative significance of under-ice data in reproducing ocean conditions, advocating for their increased use to achieve a better Southern Ocean observing system.

## Hosted file

981920\_0\_art\_1\_s5mrlq.docx available at <https://authorea.com/users/534208/articles/693705-monthly-climatology-of-the-southern-ocean-under-sea-ice>

## Hosted file

981920\_0\_supp\_11678083\_s5hxdv.docx available at <https://authorea.com/users/534208/articles/693705-monthly-climatology-of-the-southern-ocean-under-sea-ice>

## Monthly Climatology of the Southern Ocean under Sea Ice

Kaihe Yamazaki<sup>1,2</sup>, Helen Phillips<sup>1,2,3</sup>, Maxim Nikurashin<sup>1,2,3</sup>, Laura Herraiz-Borreguero<sup>3,4</sup>, Paul Spence<sup>1,2,3</sup>, Nathaniel Lee Bindoff<sup>1,2,3</sup>

<sup>1</sup>Institute of Marine and Antarctic Studies, University of Tasmania, Hobart, TAS, Australia.

<sup>2</sup>Australian Centre for Excellence in Antarctic Science, Hobart, TAS, Australia.

<sup>3</sup>Australian Antarctic Program Partnership, Institute for Marine and Antarctic Studies, Hobart, TAS, Australia.

<sup>4</sup>Commonwealth Scientific Industrial Research Organization, CSIRO Environment, Hobart, TAS, Australia.

Corresponding author: Kaihe Yamazaki ([kaiheyamazaki@gmail.com](mailto:kaiheyamazaki@gmail.com)).

### Key Points:

- A multi-purpose Southern Ocean climatology including areas under sea ice is developed using a physically consistent interpolation scheme.
- The climatology outperforms other datasets in data fidelity and significantly improves thermohaline variability under the ice.
- Under-ice profiling float and biologging data prove crucial in reproducing the subpolar and continental shelf conditions, respectively.

## 22 **Abstract**

23 The advent of under-ice profiling float and biologging techniques has enabled year-round  
24 observation of the Southern Ocean and its Antarctic margin. These under-ice data are often  
25 overlooked in widely used oceanographic datasets, despite their importance in understanding the  
26 seasonality and its role in sea ice changes, bottom water formation, and glacial melt. We develop  
27 a four-dimensional climatology of the Southern Ocean (south of 40°S and above 2,000 m) using  
28 Data Interpolating Variational Analysis, which excels in multi-dimensional interpolation and  
29 consistent handling of topography and advection. The climatology captures thermohaline  
30 variability under sea ice, previously hard to obtain, and outperforms other products in data  
31 fidelity with smaller root-mean-square errors and biases. Our dataset will be instrumental for  
32 investigating seasonality and for improving ocean models. This work further highlights the  
33 quantitative significance of under-ice data in reproducing ocean conditions, advocating for their  
34 increased use to achieve a better Southern Ocean observing system.

## 35 **Plain Language Summary**

36 In the ocean close to Antarctica, measuring water temperature and salinity beneath sea ice is  
37 difficult due to the extensive ice coverage. However, it is important to develop a standard  
38 monthly-mean dataset of ocean properties under the ice to understand the ocean's seasonal cycle,  
39 which is closely related to the global climate. With the help of new tools like underwater  
40 profiling floats and marine mammals equipped with sensors, we collect ocean data throughout  
41 the year. An advanced mapping method is used to create a physically natural representation of  
42 the ocean. This new dataset provides insights that were previously hard to obtain; for example,  
43 winter ocean conditions below 100 m depth close to the Antarctic coast. The dataset will be  
44 instrumental in building our understanding of the ocean and refining our ocean models. Our  
45 results also emphasize the need for expanded use of underwater floats and biologging for a  
46 proper representation of the ocean.

47

## 48 **1 Introduction**

49 The Southern Ocean environment is driven by the seasonal cycle of sea ice and its extent.  
50 During winter, sea ice extensively covers the ocean around Antarctica, making it one of the most  
51 inaccessible regions globally. As a result, the seasonality of the ocean properties below the sea  
52 ice remains largely undocumented (Rintoul et al., 2010). In the past decade, our understanding of  
53 the inter- and intra-annual variability of surface circulation in the Southern Ocean has improved  
54 thanks to advances in satellite altimetry data processing that allow under-ice sea surface height to  
55 be determined (e.g., Armitage et al., 2018; Dotto et al., 2018; Mizobata et al., 2020; Auger et al.,

56 2021). Simultaneously, recent innovations in under-ice measurements, particularly the use of  
57 Argo floats (e.g., Klatt et al., 2007; Wong and Riser, 2011; Chamberlain et al., 2018; Oke et al.,  
58 2022) and instrumented marine mammals (e.g., Siegelman et al., 2019; McMahon et al., 2021),  
59 have facilitated ocean monitoring throughout the year. These under-ice measurements have  
60 adeptly recorded the distinct winter conditions of the Southern Ocean, specifically the surface  
61 mixed layer (Wong and Riser, 2011; Pellichero et al., 2017; Wilson et al., 2019), frontal  
62 structures (Pauthenet et al., 2021), and supercooled waters linked to sea ice formation processes  
63 (Haumann et al., 2020).

64 A prime example that underscores the importance of under-ice data is the subsurface  
65 seasonality of the Southern Ocean. This significantly affects stratification at the base of the  
66 mixed layer and the penetration of warm subsurface waters into the mixed layer, thereby  
67 influencing sea ice extent across interseasonal timescales (Wilson et al., 2019; Doddridge et al.,  
68 2021; Libera et al., 2022). The freshwater flux mediated by sea ice plays a fundamental role in  
69 the upper branch of the meridional overturning circulation (Abernathey et al., 2016; Haumann et  
70 al., 2016; Pellichero et al., 2018). Furthermore, our understanding of the long-term trends in  
71 Antarctic and Southern Ocean water masses has primarily been derived from summer data  
72 (Schmidtko et al., 2014; Yamazaki et al., 2021; Herraiz-Borreguero and Naveira Garabato,  
73 2022). Atmospheric trends over the Southern Ocean have a distinct seasonal asymmetry, such as  
74 the summer-biased strengthening of the Southern Annular Mode (Hazel et al., 2019; Neme et al.,  
75 2022; Fraser and Wongpan et al., 2023). The seasonally asymmetric trends are likely key in  
76 triggering the climatic regime shift in the Southern Ocean and Antarctica (Herraiz-Borreguero  
77 and Naveira Garabato, 2022; Purich and Doddridge, 2023; King et al., 2023). These factors

78 motivate the need for a standard monthly climatology of the Southern Ocean interior that extends  
79 beneath the sea ice.

80         The task of curating and analyzing under-ice data currently poses significant challenges  
81 for a large portion of the scientific community. Consequently, this barrier can lead to  
82 misrepresentation in ocean models and thus inaccurate predictions for changes in climate and sea  
83 level. One critical reason for the underutilization of under-ice Argo float is the absence of  
84 position information. Position data are only available when floats surface in ice-free ocean areas.  
85 Under sea ice, float positions are inferred by interpolating between two surface locations in a  
86 straight line or along a dynamically-consistent path, in which positional errors are typically  
87 around 50 km (Chamberlain et al., 2018; Yamazaki et al., 2020; Oke et al., 2022). Around 40%  
88 of the Argo profiles collected in the Southern Ocean seasonal ice zone are flagged as under ice  
89 (Yamazaki et al., 2020). The Argo float constitutes the most significant portion of profile  
90 numbers in the ocean interior, while biologging data dominate the profile numbers near the  
91 Antarctic margin (e.g., Pauthenet et al., 2021). Despite the abundance of the under-ice profiles in  
92 the Southern Ocean, they have not been included in major datasets such as the NOAA World  
93 Ocean Database (<https://www.ncei.noaa.gov>) and the Hadley Centre EN4  
94 (<https://www.metoffice.gov.uk/>), which are commonly used for initializing climate models. No  
95 existing climatology product includes both under-ice Argo and biologging data except in specific  
96 applications for physical oceanography investigations (e.g., Pellichero et al., 2017; Pauthenet et  
97 al., 2021). This is despite increasing demands for these data to be used in high-resolution ocean  
98 modelling and ocean biogeochemistry studies at the Antarctic margin.

99         In this study, we develop a novel four-dimensional monthly climatology of the Southern  
100 Ocean that includes the under-ice data. Historically, various methods have been employed to

101 map oceanographic properties in the Southern Ocean, such as optimal interpolation with  
102 topographic constraints (Ridgway et al., 2002; Shimada et al., 2017; Mensah and Ohshima,  
103 2023), fast-marching algorithm (Schmidtko et al., 2013; 2014), and several machine learning  
104 techniques (Giglio et al., 2018; Yamazaki et al., 2020; Pauthenet et al., 2021; Sonnewald et al.,  
105 2023). The present study adopts the Data Interpolating Variational Analysis (DIVA; Barth et al.,  
106 2014; Roach and Bindoff, 2023), which offers enhanced capabilities in handling topographic and  
107 advection constraints, multi-dimensional interpolation (including time), and superior statistical  
108 performance compared to conventional methods (see Section 2.2 and Text S1 for details). Our  
109 analysis incorporates both under-ice Argo and biologging data as performed in Pauthenet et al.  
110 (2021), but extends northward to 40°S and downward to 2,000 dbar with a finer horizontal  
111 resolution. We juxtapose our results with the latest version of World Ocean Atlas (WOA23;  
112 Regan et al., 2023; Locarnini et al., 2023) and the Southern Ocean State Estimate integrated with  
113 biogeochemical components (B-SOSE; Verdy and Mazloff, 2017). The B-SOSE solution is  
114 eddy-permitting and adjusted to observations by tuning model parameters and boundary  
115 conditions.

116 This paper is structured as follows: Section 2 details the data and methods used for the  
117 monthly climatology with the DIVA interpolation. Section 3 presents the interpolated  
118 climatology and compares it to the other datasets. Section 4 provides the conclusions. In this  
119 paper, we present a succinct overview of the subsurface seasonality. Given its relevance to a  
120 broad spectrum of scientific interests and perspectives, it warrants more extensive investigation.

121

## 122 **2 Data and Methods**

## 123 2.1 Input data

124 Conductivity-Temperature-Depth (CTD) profiles from multiple instrument types are  
125 collected: the Argo float (Argo, 2000; Wong et al., 2020), biologging data from instrumented  
126 seals (MEOP; Roquet et al., 2021; McMahon et al., 2021), and ship-based measurements  
127 available in the World Ocean Database (Boyer et al., 2018). The collected observations are  
128 overviewed in Figure 1a and 1b. The treatment for the quality flags and the under-ice Argo data  
129 is noted in Text S2. The collected profiles span the period from 1910 to 2023. As shown by  
130 Pauthenet et al. (2021), there is a notable observation density bias toward the period post-2005,  
131 primarily due to the prevalence of Argo and biologging profiles. Consequently, the resulting  
132 climatology is predominantly representative of this recent timeframe. From the CTD profiles, we  
133 extract surface data for temperature and salinity across the interpolating layers using Akima  
134 interpolation at 1 m intervals.

135 The additional input data for DIVA are outlined in Figure S1. The International  
136 Bathymetric Chart of the Southern Ocean, version 2 (IBCSOv2; Dorschel et al., 2022), provides  
137 the topographic constraint. The horizontal correlation scale is proportionally aligned with the  
138 bathymetric gradient, which is then mapped onto the interpolation grid. For the advection  
139 constraint, we use the climatological velocity from B-SOSE iteration 136 (Figure S2a). An  
140 assessment of this advection constraint can be found in Text S5. The background field for DIVA  
141 temperature and salinity is derived from the climatological field of WOA23. This implies that the  
142 temporal variation in the derived field (e.g., Figure S9a) is based solely on the collected CTD  
143 profiles, while the spatial variation is somewhat influenced by WOA23. Further details about the  
144 input data are provided in Text S2.

## 145 2.2 Data Interpolating Variational Analysis

146 We employ the multidimensional DIVA implemented by a Julia package DIVAnd (Barth  
147 et al., 2014), which facilitates the semi-automatic calibration of tuning parameters. As in Roach  
148 and Bindoff (2023), we perform three-dimensional DIVA in horizontal/time dimensions and  
149 iterate the process across vertical layers to construct the four-dimensional climatology. In the  
150 version of the climatology released with this paper (2023.11), the dataset covers 66 layers  
151 ranging from 5 to 2,000 m, following the standard levels of WOA23. The interpolation grids are  
152 circumpolar between 75°S to 40°S with grid intervals set at 1/2° in longitude, 1/4° in latitude and  
153 monthly in time. This horizontal grid configuration results in an approximate 25 km interval at  
154 60°S, which appears adequate to smoothly capture the synoptic-scale variability (e.g., Auger et  
155 al., 2022).

156 To optimize the analysis for the Antarctic margin, interpolation tests are conducted south  
157 of 50°S (detailed in Text S3). Based on these tests, we determine the relative correlation time  
158 scale and advection weighting (see also Figure S1). Simultaneously, the correlation scaling factor  
159 and smoothing factor (signal-to-noise ratio) are automatically calibrated using the cross-  
160 validation function (Troupin et al., 2012), which aims to minimize data residuals and  
161 interpolation biases. By multiplying the relative correlation scales in space and time with the  
162 correlation scaling factor, we determined the correlation time scale to be 1.86 months, and the  
163 horizontal correlation scale to range between 100 and 400 km (see Figure S2). This calibrated  
164 correlation scale broadly aligns with findings from previous studies on optimal interpolation  
165 (Shimada et al., 2017) and model analysis (Mazloff et al., 2018; Auger et al., 2022).

166           The interpolation error linked with DIVA is estimated using the approximation method in  
167 Beckers et al. (2014), a feature integrated into the DIVAnd package. This interpolation error  
168 tends to escalate in areas where data is sparser, both spatially and temporally (Figure 1d). As  
169 detailed in Text S4, potential error associated with spatial smoothing due to the nonlinear nature  
170 of the equation of state (known as cabbeling) can be crudely corrected using the standard  
171 deviation of temperature and salinity following the method in Schmidtko et al. (2013). More  
172 information about the procedure of DIVA can be found in Supporting Information.

### 173 **3 Results**

#### 174 3.1 Interpolated field

175           In Figure 1, the data distribution by platform, observed temperature at 100 m, and the  
176 DIVA-interpolated temperature are presented for March, June, September, and December. The  
177 DIVA field accurately reproduces the nuances of the original observations, as illustrated in  
178 Figures 1b and 1c. Interpolation error can become significantly large over the continental shelf  
179 due to data scarcity (Figure 1d), so that areas with an interpolation error over 1°C have been  
180 masked out in Figure 1c. Conversely, areas with abundant data exhibit small interpolation errors.  
181 In these regions, a large standard deviation indicates substantial spatiotemporal variation, likely  
182 corresponding to significant horizontal gradients in temperature or salinity. The DIVA field and  
183 observational data are further compared in time series in Figure S5, demonstrating how the  
184 sparsity and dispersion of observations relate to the interpolation error and standard deviation.  
185 Both variables serve as statistical measures for assessing the DIVA interpolation. As depicted in  
186 Figure S9a, the DIVA field captures the widespread seasonal variation of the 100 m temperature

187 by up to 1°C, which has not necessarily been evident in other datasets. Monthly maps of the  
188 interpolated temperature and salinity from 5 to 2,000 m are available in Movie S1.

189 As a result of the semi-automatic calibration of the tuning parameters, the misfit of the  
190 DIVA field from observations is very small. South of 60°S (i.e., the southern part of the  
191 interpolation test domain; Section 2.2), the root-mean-square error of annual mean potential  
192 temperature at 100 m is estimated to be 0.492°C, and the bias is less than 0.000°C. For salinity at  
193 100 m, the root-mean-square error is 0.089 psu, and the bias is less than 0.000 psu. Crucially,  
194 these statistics outperform those of WOA23 and the B-SOSE monthly climatology as shown in  
195 Section 3.2).

### 196 3.2 Comparison with other datasets

197 Figure 2 compares the DIVA temperature at 100 m in March and September with the  
198 corresponding data from WOA23, which does not include biologging data, and with the monthly  
199 climatology derived from the B-SOSE iteration 136. The B-SOSE solution spans from 2013 to  
200 2021. Constructing the DIVA using observations over the same period shows that the difference  
201 in time period does not affect the following comparison. In Figure 2, areas with large  
202 interpolation error are not masked, since the corresponding error estimate — expected to be  
203 larger in areas with sparse observations — is unavailable in both WOA23 and B-SOSE.

204 DIVA and WOA23 are consistent on the basin-scale temperature variations (Figures 2a  
205 and 2b), while noticeable differences in nuances are observed on smaller scales. Generally,  
206 DIVA is smoother than WOA23. For instance, in September, WOA23 depicts warm blobs  
207 crossing the continental slopes (indicated by black arrows) and forming spotty patterns offshore  
208 (indicated by a white arrow). Despite the potential for spurious interpolation due to data scarcity

209 during the freezing season, DIVA successfully derives a physically consistent field. Meanwhile,  
210 the B-SOSE temperature is significantly warmer than the DIVA field in both March and  
211 September (by around 1°C; see also Figure S8), indicating relatively large biases in the model  
212 solution.

213 In WOA23 and B-SOSE, the misfit from the observations is generally larger than that for  
214 the DIVA product. South of 60°S, the root-mean-square error increases to 0.587°C for WOA23  
215 and 1.307°C for B-SOSE, and the bias increases to -0.013°C and 0.657°C, respectively (Figure  
216 2d). The data fidelity of DIVA is further highlighted when focusing on specific periods or areas  
217 with a limited number of data points, such as in September (Figure 2e) and on the continental  
218 shelf (Figure 2f). In these cases, the root-mean-square error/bias differences from DIVA to the  
219 two datasets become more pronounced than in the annual mean south of 60°S (Figure 2d). A  
220 similar discussion can be derived from the comparison in salinity at 100 m (Figure S7).

221 The vertical structure is summarised in zonally-averaged meridional sections (Figure 3).  
222 The standard deviation of temperature and salinity, indicative of the strength of seasonal  
223 variation, demonstrates surface-originated seasonality in all datasets. The penetration of this  
224 seasonality is typically characterised by the extent of winter water below 0°C. WOA23 exhibits a  
225 zonally-averaged structure similar to that of DIVA, but has less smoothed features (Figure 2b,  
226 arrows) that result in greater subsurface seasonal variation than in DIVA (Figures 3a, 3b and 3d).  
227 The 100 m temperature difference from DIVA (Figure S8b) and the difference in the monthly  
228 temperature anomalies (Figures S9a and S9b) are also related to this discrepancy.

229 The seasonality of B-SOSE does not extend as deeply as in the DIVA field (Figures 3a,  
230 3c), and the difference in the annual-mean temperature (Figure 3e, top panel) shows a positive

231 peak around 100 m that connects to deeper layers in the north where B-SOSE is much warmer  
232 than DIVA. The salinity plots are largely a mirror image of temperature, with B-SOSE being  
233 much fresher than DIVA toward the surface. The B-SOSE and the DIVA fields have relatively  
234 good agreement in near-surface temperature. The discrepancy in subsurface temperature is thus  
235 likely related to the modeled mixed layer depth and winter water. The reason for this  
236 misrepresentation could be linked to the near-surface fresh bias. The fresh surface layer can act  
237 as a barrier to surface mixing, leading to shallow winter convection and warm bias at depth. The  
238 DIVA climatology and the presented datasets are further assessed in Text S5.

### 239 3.3 Effect of including under-ice data

240 To quantify the importance of under-ice data, two additional DIVA fields are constructed,  
241 one excluding under-ice Argo data (“no-iceArgo”) and the other excluding bioglogging data (“no-  
242 MEOP”). Their temperature differences compared to the referential DIVA at 100 m are shown in  
243 Figure 4, characterising the effect of including these data in capturing the seasonality. Inclusion  
244 of the under-ice Argo data results in changes in the DIVA temperature by  $\sim 1^\circ\text{C}$  in June and  
245 September, while also significantly reducing the interpolation error by more than  $1^\circ\text{C}$  (Figures  
246 4a and 4b). This effect stands out clearly along the Antarctic margin, between the climatological  
247 sea ice extent maxima and the continental slope isobath.

248 In contrast, the inclusion of bioglogging data has a noticeable effect over the continental  
249 shelf (Figures 4c and 4d). There, its influence on the DIVA temperature and the interpolation  
250 error is found to be comparable in magnitude to the influence of the under-ice Argo data.  
251 Although this effect may be relevant to the observed differences between the reference DIVA  
252 and WOA23 (Figure S8b), as the latter does not include the bioglogging data, there is no clear

253 correlation. The significant impacts of incorporating under-ice Argo data and biologging data in  
254 the different areas highlight their irreplaceable roles in reproducing the seasonality of the  
255 Southern Ocean and the oceanic conditions under sea ice.

## 256 **4 Conclusions**

257 Historically, under-ice measurements in the Southern Ocean have been hindered by the  
258 extensive presence of sea ice. Under the current climate of rapid change in the ocean and ice  
259 around Antarctica, it is crucial to have a monthly climatology that covers beneath the sea ice to  
260 answer questions related to the seasonal variability (e.g., of air-sea-ice interaction and ocean heat  
261 transport). However, no multi-purpose monthly climatology focusing on the under-ice Southern  
262 Ocean has been made due to the challenges in curating and combining under-ice data from  
263 various platforms. This barrier to under-ice data observations has been a significant obstacle in  
264 assessing performance of ocean models particularly during the freezing season, potentially  
265 leading to inaccurate climate predictions.

266 In this study, we have developed a monthly climatology of the Southern Ocean that  
267 incorporates both under-ice Argo and biologging data. We used the DIVA scheme, an advanced  
268 type of conventional optimal interpolation that enables a relatively simple multi-dimensional  
269 interpolation and handling of topographic and advection constraints. By maintaining physical  
270 consistency and data fidelity, our climatology successfully captures the subsurface seasonality  
271 more accurately, a feature previously challenging to reproduce in other climatologies and state  
272 estimate simulations. Furthermore, the comparison between the referential climatology and the  
273 climatology excluding under-ice data revealed that the inclusion of under-ice data alters the 100-  
274 m temperature by approximately 1°C and decreases the interpolation error by more than 1°C.

275 The under-ice Argo data are crucial for accurately representing the subpolar Southern Ocean  
276 during winter, and the biologging data are essential for accurately representing ocean conditions  
277 over the continental shelf. This result represents the first quantification of the effect of under-ice  
278 data on constructing a climatological dataset.

279 Our results underscore the critical need for expanding the use of both under-ice Argo  
280 floats and biologging techniques to improve monitoring of the Southern Ocean. Argo is currently  
281 adapting its global coverage plan to include polar regions and marginal seas (as part of Polar  
282 Argo), areas that were initially excluded from the original design due to technological  
283 constraints. In conjunction with ship-based measurements, which will remain an essential  
284 observation platform in the Antarctic margin heavily covered by sea ice, these autonomous  
285 observation techniques provide unique and complementary contributions to the complete  
286 coverage. The integration of these different platforms is expected to occur through close  
287 communication via the Southern Ocean Observing System (SOOS; Rintoul et al., 2010; Newman  
288 et al., 2019) and the Global Ocean Observing System (GOOS).

## 289 **Acknowledgments**

290 We thank Christopher Roach and Matthias Auger for valuable comments. This research was  
291 supported by the Australian Research Council Special Research Initiative, Australian Centre for  
292 Excellence in Antarctic Science (Project Number SR200100008) and by the Australian  
293 Government as part of the Antarctic Science Collaboration Initiative. Computational resources  
294 for the SOSE were provided by NSF XSEDE resource grant OCE130007 and NSF award PLR-  
295 1425989. Among contributions to the International Argo Program by several countries and  
296 programs, we especially thank the SOCCOM program.

## 297 **Open Research**

298 The Southern Ocean monthly climatology presented in this study is open to the public via  
299 Zenodo (<https://doi.org/10.5281/zenodo.10350472>). The Argo data were collected and made  
300 freely available by the International Argo Program (<http://www.argo.ucsd.edu>,  
301 <https://www.euro-argo.eu>). The bioglogging data were made freely available by the International  
302 MEOP Consortium and the AniBOS network (<http://www.meop.net>). World Ocean Database  
303 and World Ocean Atlas are available from National Centers for Environmental Information,  
304 NOAA (<https://www.ncei.noaa.gov>). B-SOSE solutions are publicly available from University of  
305 California, San Diego (<http://sose.ucsd.edu>). Julia package DIVAnd is accessible via GitHub  
306 (<https://github.com/gher-uliege/DIVAnd.jl>).

307

## 308 **References**

- 309 1. Abernathey, R. P., Cerovecki, I., Holland, P. R., Newsom, E., Mazloff, M., & Talley, L. D. (2016).  
310 Water-mass transformation by sea ice in the upper branch of the Southern Ocean overturning. *Nature*  
311 *Geoscience*, 9(8), 596-601.
- 312 2. Argo (2000). Argo float data and metadata from Global Data Assembly Centre (Argo GDAC).  
313 SEANOE. <https://doi.org/10.17882/42182>
- 314 3. Armitage, T. W., Kwok, R., Thompson, A. F., & Cunningham, G. (2018). Dynamic topography and  
315 sea level anomalies of the Southern Ocean: Variability and teleconnections. *Journal of Geophysical*  
316 *Research: Oceans*, 123(1), 613-630.
- 317 4. Auger, M., Prandi, P., & Sallée, J. B. (2022). Southern ocean sea level anomaly in the sea ice-covered  
318 sector from multimission satellite observations. *Scientific Data*, 9(1), 70.
- 319 5. Barth, A., Beckers, J. M., Troupin, C., Alvera-Azcárate, A., & Vandenbulcke, L. (2014). divand-1.0:  
320 n-dimensional variational data analysis for ocean observations. *Geoscientific Model Development*,  
321 7(1), 225-241.

- 322 6. Beckers, J. M., Barth, A., Troupin, C., & Alvera-Azcárate, A. (2014). Approximate and efficient  
323 methods to assess error fields in spatial gridding with data interpolating variational analysis (DIVA).  
324 *Journal of Atmospheric and Oceanic Technology*, 31(2), 515-530.
- 325 7. Boyer, T.P., Baranova, O.K., Coleman, C., Garcia, H.E., Grodsky, A., Locarnini, R.A., Mishonov,  
326 A.V., Paver, C.R., Reagan, J.R., Seidov, D., Smolyar, I.V., Weathers, K., & Zweng, M.M. (2018).  
327 *World Ocean Database 2018*. In A.V. Mishonov (Tech. Ed.), NOAA Atlas NESDIS 87.
- 328 8. Chamberlain, P. M., Talley, L. D., Mazloff, M. R., Riser, S. C., Speer, K., Gray, A. R., &  
329 Schwartzman, A. (2018). Observing the ice-covered Weddell Gyre with profiling floats: Position  
330 uncertainties and correlation statistics. *Journal of Geophysical Research: Oceans*, 123(11), 8383-8410.
- 331 9. Doddridge, E. W., Marshall, J., Song, H., Campin, J. M., & Kelley, M. (2021). Southern Ocean heat  
332 storage, reemergence, and winter sea ice decline induced by summertime winds. *Journal of Climate*,  
333 34(4), 1403-1415.
- 334 10. Dorschel, B., Hehemann, L., Viquerat, S., Warnke, F., Dreutter, S., Tenberge, Y. S., ... & Arndt, J. E.  
335 (2022). The international bathymetric chart of the southern ocean version 2. *Scientific data*, 9(1), 275.
- 336 11. Dotto, T. S., Naveira Garabato, A. C., Bacon, S., Tsamados, M., Holland, P. R., Hooley, J., et al.  
337 (2018). Variability of the Ross Gyre, Southern Ocean: Drivers and responses revealed by satellite  
338 altimetry. *Geophysical Research Letters*, 45, 6195–6204.
- 339 12. Giglio, D., Lyubchich, V., & Mazloff, M. R. (2018). Estimating oxygen in the Southern Ocean using  
340 argo temperature and salinity. *Journal of Geophysical Research: Oceans*, 123(6), 4280-4297.
- 341 13. Haumann, F. A., Moorman, R., Riser, S. C., Smedsrud, L. H., Maksym, T., Wong, A. P., ... &  
342 Sarmiento, J. L. (2020). Supercooled Southern Ocean waters. *Geophysical Research Letters*, 47(20),  
343 e2020GL090242.
- 344 14. Haumann, F. A., Gruber, N., Münnich, M., Frenger, I., & Kern, S. (2016). Sea-ice transport driving  
345 Southern Ocean salinity and its recent trends. *Nature*, 537(7618), 89-92.
- 346 15. Hazel, J. E., & Stewart, A. L. (2019). Are the near-Antarctic easterly winds weakening in response to  
347 enhancement of the southern annular mode?. *Journal of Climate*, 32(6), 1895-1918.

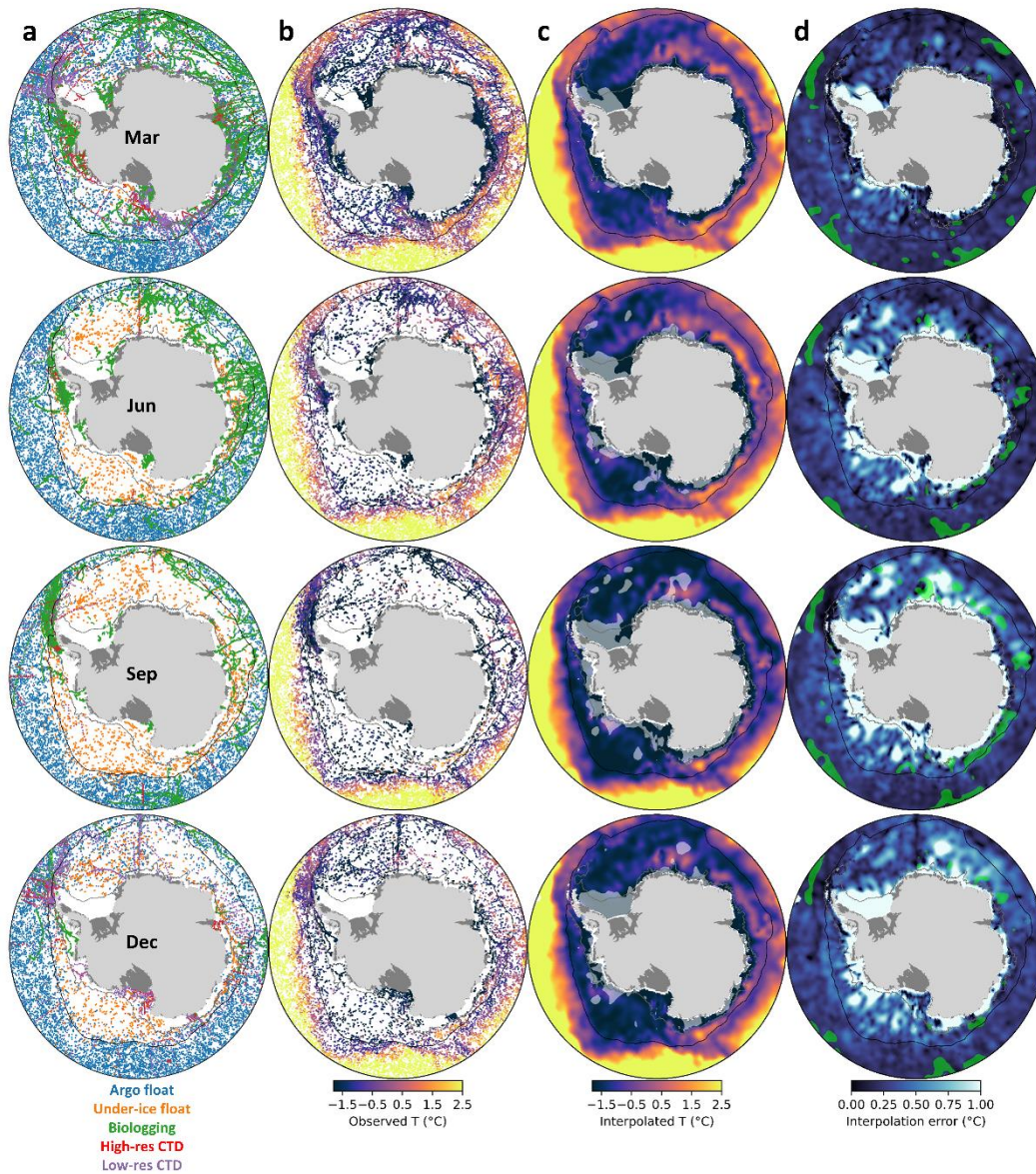
- 348 16. King, M. A., Lyu, K., & Zhang, X. (2023). Climate variability a key driver of recent Antarctic ice-  
349 mass change. *Nature Geoscience*, 1-8.
- 350 17. Klatt, O., Boebel, O., & Fahrbach, E. (2007). A profiling float's sense of ice. *Journal of Atmospheric*  
351 *and Oceanic Technology*, 24(7), 1301-1308.
- 352 18. Locarnini, R. A., O. K. Baranova, A. V. Mishonov, T. P. Boyer, J. R. Reagan, D. Dukhovskoy, D.  
353 Seidov, H. E. Garcia, C. Bouchard, S. Cross, C. R. Paver, and Z. Wang, 2023. *World Ocean Atlas*  
354 *2023, Volume 1: Temperature*. A. Mishonov Technical Ed. NOAA Atlas NESDIS (in preparation).
- 355 19. McMahon, C. R., Roquet, F., Baudel, S., Belbeoch, M., Bestley, S., Blight, C., ... & Woodward, B.  
356 (2021). Animal borne ocean sensors—AniBOS—An essential component of the global ocean observing  
357 system. *Frontiers in Marine Science*, 8, 751840.
- 358 20. Mazloff, M. R., Cornuelle, B. D., Gille, S. T., & Verdy, A. (2018). Correlation lengths for estimating  
359 the large-scale carbon and heat content of the Southern Ocean. *Journal of Geophysical Research:*  
360 *Oceans*, 123(2), 883-901.
- 361 21. Mensah, V., & Ohshima, K. I. (2023). A mapping methodology adapted to all polar and subpolar  
362 oceans with a stretching/shrinking constraint. *Journal of Atmospheric and Oceanic Technology*,  
363 40(10), 1241-1261.
- 364 22. Naveira Garabato, A. C., Dotto, T. S., Hooley, J., Bacon, S., Tsamados, M., Ridout, A., Frajka-  
365 Williams, E. E., Herraiz-Borreguero, L., Holland, P. R., Heorton, H. D. B. S. and Meredith, M. P.  
366 (2019). Phased response of the subpolar Southern Ocean to changes in circumpolar winds.  
367 *Geophysical Research Letters*, 46, 6024–6033.
- 368 23. Neme, J., England, M. H., & McC. Hogg, A. (2022). Projected changes of surface winds over the  
369 Antarctic continental margin. *Geophysical Research Letters*, 49(16), e2022GL098820.
- 370 24. Newman, L., Heil, P., Trebilco, R., Katsumata, K., Constable, A., Van Wijk, E., ... & Spreen, G.  
371 (2019). Delivering sustained, coordinated, and integrated observations of the Southern Ocean for  
372 global impact. *Frontiers in Marine Science*, 6, 433.
- 373 25. Oke, P. R., Rykova, T., Pilo, G. S., & Lovell, J. L. (2022). Estimating Argo float trajectories under  
374 ice. *Earth and Space Science*, 9(7), e2022EA002312.

- 375 26. Pauthenet, E., Sallée, J. B., Schmidtko, S., & Nerini, D. (2021). Seasonal variation of the Antarctic  
376 Slope Front occurrence and position estimated from an interpolated hydrographic climatology. *Journal*  
377 *of Physical Oceanography*, 51(5), 1539-1557.
- 378 27. Pellichero, V., Sallée, J. B., Schmidtko, S., Roquet, F., & Charrassin, J. B. (2017). The ocean mixed  
379 layer under Southern Ocean sea-ice: Seasonal cycle and forcing. *Journal of Geophysical Research:*  
380 *Oceans*, 122(2), 1608-1633.
- 381 28. Pellichero, V., Sallée, J. B., Chapman, C. C., & Downes, S. M. (2018). The southern ocean meridional  
382 overturning in the sea-ice sector is driven by freshwater fluxes. *Nature communications*, 9(1), 1789.
- 383 29. Purich, A., & Doddridge, E. W. (2023). Record low Antarctic sea ice coverage indicates a new sea ice  
384 state. *Communications Earth & Environment*, 4(1), 314.
- 385 30. Roach, C. J., & Bindoff, N. L. (2023). Developing a New Oxygen Atlas of the World's Oceans Using  
386 Data Interpolating Variational Analysis. *Journal of Atmospheric and Oceanic Technology*, 40(11),  
387 1475-1491.
- 388 31. Reagan, J. R., D. Dukhovskoy, D. Seidov, T. P. Boyer, R. A. Locarnini, O. K. Baranova, A. V.  
389 Mishonov, H. E. Garcia, C. Bouchard, S. Cross, C. R. Paver, and Z. Wang (2023). *World Ocean Atlas*  
390 *2023, Volume 2: Salinity*. A. Mishonov Technical Ed. NOAA Atlas NESDIS (in preparation).
- 391 32. Ridgway, K. R., Dunn, J. R., & Wilkin, J. L. (2002). Ocean interpolation by four-dimensional  
392 weighted least squares—Application to the waters around Australasia. *Journal of atmospheric and*  
393 *oceanic technology*, 19(9), 1357-1375.
- 394 33. Rintoul, S. R., Speer, K., Sparrow, M., Meredith, M., Hofmann, E., Fahrbach, E., ... & Gladyshev, S.  
395 (2010). Southern Ocean Observing System (SOOS): Rationale and strategy for sustained observations  
396 of the Southern Ocean. *Proceedings of OceanObs '09: Sustained Ocean Observations and Information*  
397 *for Society*.
- 398 34. Roquet, F., Guinet, C., Charrassin, J.-B., Costa, D. P., Kovacs, K. M., Lydersen, C., Bornemann, H.,  
399 Bester, M. N., Muelbert, M. C., Hindell, M. A., McMahon, C. R., Harcourt, R., Boehme, L., & Fedak,  
400 M. A. (2021). MEOP-CTD in-situ data collection: A Southern ocean Marine-mammals calibrated sea  
401 water temperatures and salinities observations. SEANOE. <https://doi.org/10.17882/45461>

- 402 35. Roemmich, D. and J. Gilson (2009), The 2004-2008 mean and annual cycle of temperature, salinity,  
403 and steric height in the global ocean from the Argo Program. *Progress in Oceanography*, 82, 81-100.
- 404 36. Schmidtko, S., Johnson, G. C., & Lyman, J. M. (2013). MIMOC: A global monthly isopycnal upper-  
405 ocean climatology with mixed layers. *Journal of Geophysical Research: Oceans*, 118(4), 1658-1672.
- 406 37. Schmidtko, S., Heywood, K. J., Thompson, A. F., & Aoki, S. (2014). Multidecadal warming of  
407 Antarctic waters. *Science*, 346(6214), 1227-1231.
- 408 38. Shimada, K., Aoki, S., & Ohshima, K. I. (2017). Creation of a gridded dataset for the southern ocean  
409 with a topographic constraint scheme. *Journal of Atmospheric and Oceanic Technology*, 34(3), 511-  
410 532.
- 411 39. Siegelman, L., Roquet, F., Mensah, V., Rivière, P., Pauthenet, E., Picard, B., & Guinet, C. (2019).  
412 Correction and accuracy of high-and low-resolution CTD data from animal-borne instruments. *Journal*  
413 *of Atmospheric and Oceanic Technology*, 36(5), 745-760.
- 414 40. Sonnewald, M., Reeve, K. A., & Lguensat, R. (2023). A Southern Ocean supergyre as a unifying  
415 dynamical framework identified by physics-informed machine learning. *Communications Earth &*  
416 *Environment*, 4(1), 153.
- 417 41. Troupin, C., Barth, A., Sirjacobs, D., Ouberdous, M., Brankart, J. M., Brasseur, P., ... & Beckers, J.  
418 M. (2012). Generation of analysis and consistent error fields using the Data Interpolating Variational  
419 Analysis (DIVA). *Ocean Modelling*, 52, 90-101.
- 420 42. Verdy, A., & Mazloff, M. R. (2017). A data assimilating model for estimating Southern Ocean  
421 biogeochemistry. *Journal of Geophysical Research: Oceans*, 122(9), 6968-6988.
- 422 43. Wilson, E. A., Riser, S. C., Campbell, E. C., & Wong, A. P. (2019). Winter upper-ocean stability and  
423 ice–ocean feedbacks in the sea ice–covered Southern Ocean. *Journal of Physical Oceanography*,  
424 49(4), 1099-1117.
- 425 44. Wong, A. P. S., et al. (2020). Argo Data 1999–2019: Two Million Temperature-Salinity Profiles and  
426 Subsurface Velocity Observations From a Global Array of Profiling Floats. *Frontiers in Marine*  
427 *Science*, 7(700). <https://doi.org/10.3389/fmars.2020.00700>

- 428 45. Yamazaki, K., Aoki, S., Shimada, K., Kobayashi, T., & Kitade, Y. (2020). Structure of the subpolar  
429 gyre in the Australian-Antarctic Basin derived from Argo floats. *Journal of Geophysical Research:*  
430 *Oceans*, 125(8), e2019JC015406.
- 431 46. Yamazaki, K., Aoki, S., Katsumata, K., Hirano, D., & Nakayama, Y. (2021). Multidecadal poleward  
432 shift of the southern boundary of the Antarctic Circumpolar Current off East Antarctica. *Science*  
433 *advances*, 7(24), eabf8755.
- 434

435

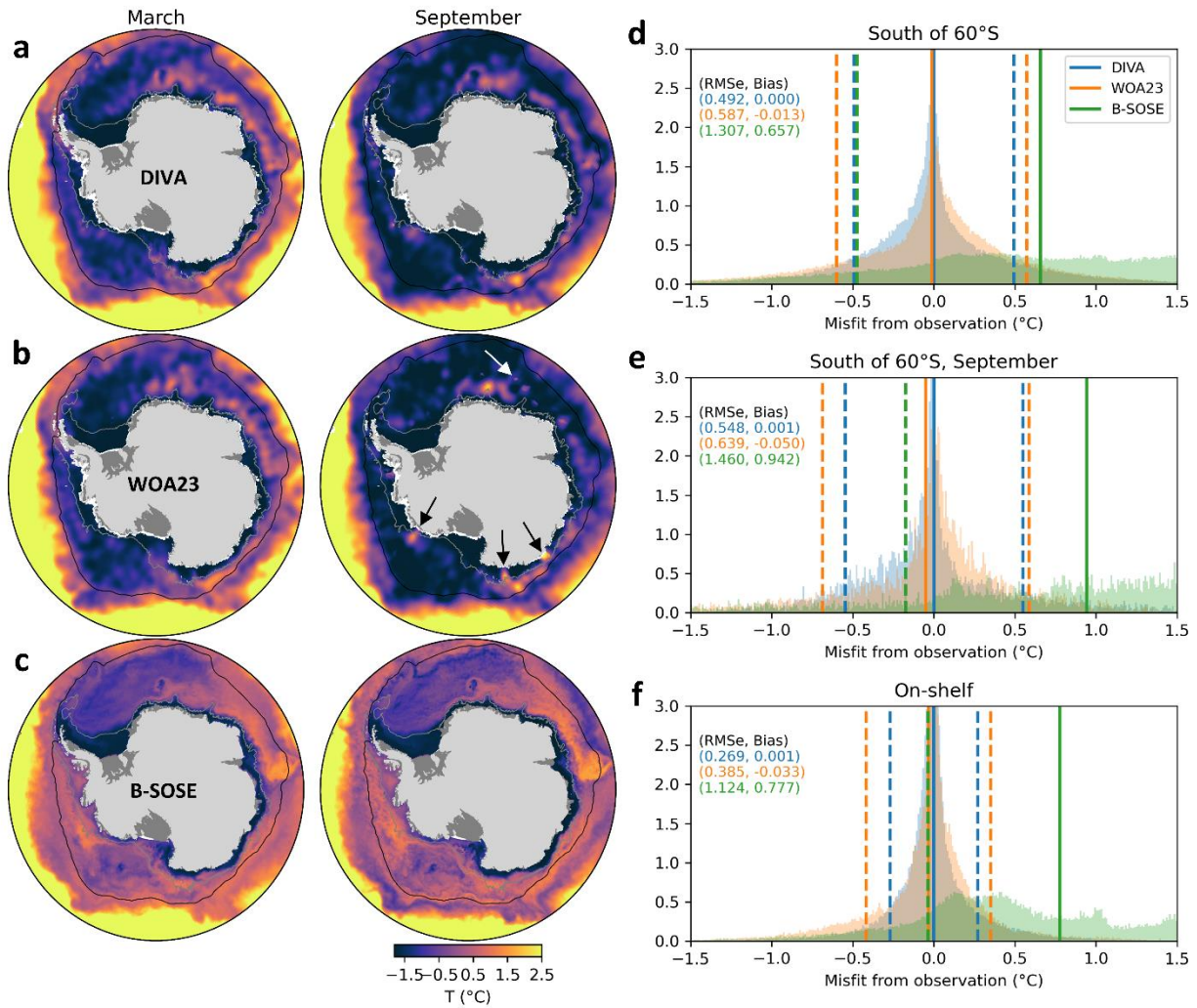


436

437

438 **Figure 1.** Observations and interpolated fields for March, June, September, and December by  
 439 row. Columns are: (a) data population colored by platform type. (b) Temperature at 100 m, as  
 440 measured from in-situ observations. (c) DIVA-interpolated temperature at 100 m; areas with  
 441 interpolation errors larger than 1°C are masked in gray. (d) Interpolation errors in °C. Standard  
 442 deviation larger than 1 °C is shown in green. The black line represents the climatological sea ice  
 443 extent in September, defined by a 15% sea ice concentration (sourced from NSIDC), as the  
 444 boundary of the seasonal ice zone. The 3,000 m isobath of the continental slope is shown in gray.  
 445

446



447

448

449

450

451

452

453

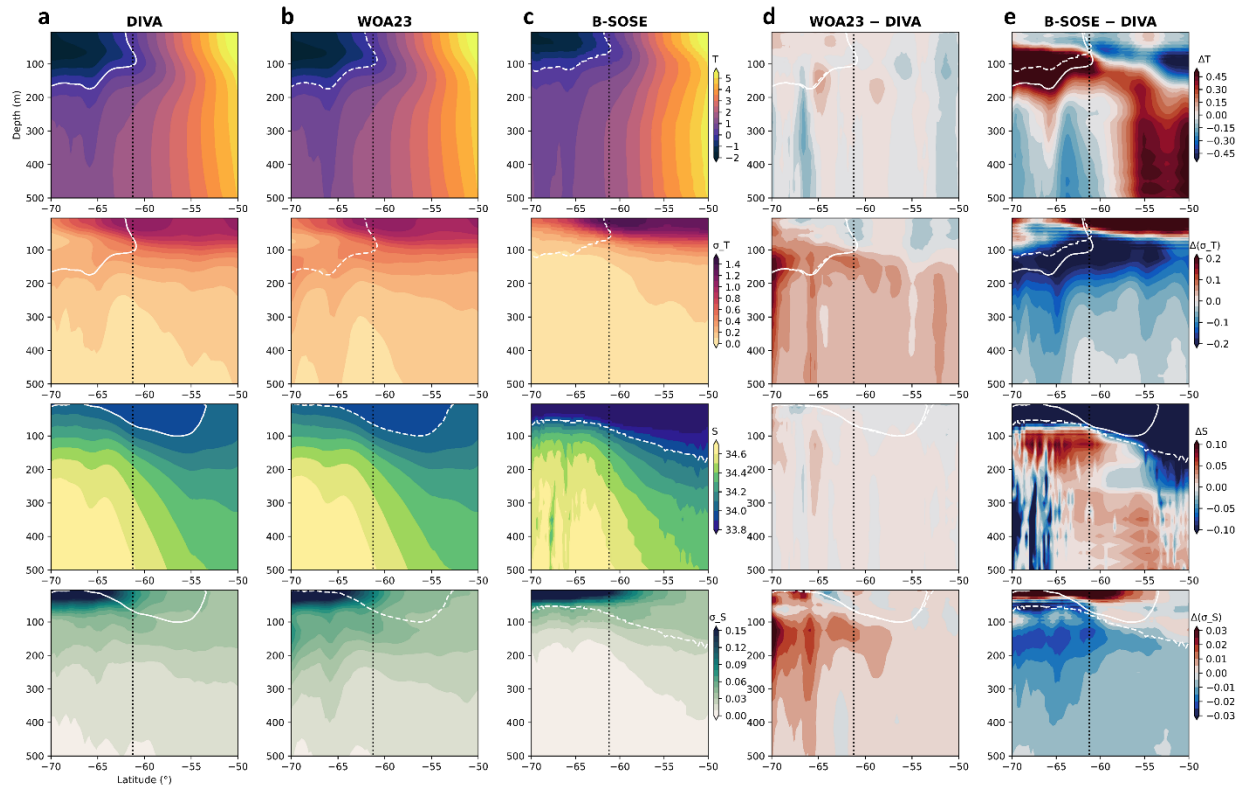
454

455

456

**Figure 2.** Comparison between three datasets. Monthly-mean temperature at 100 m is shown for (a) DIVA, (b) WOA23, and (c) B-SOSE in March (left) and September (right). In panel (b), spurious features in September are annotated by white and black vectors. (d) Histogram of misfit from observation for 100 m temperature by all available data south of 60°S (blue: DIVA, orange: WOA23, green: B-SOSE). Root-mean-square errors and biases are shown in upper-left figures in the corresponding color and plotted as broken and solid lines, respectively. Data from September (e) and data from the continental shelf defined by sea depths shallower than 1,000 m (f) are also presented. Bin size of histogram is set to 0.01  $^{\circ}\text{C}$ .

457



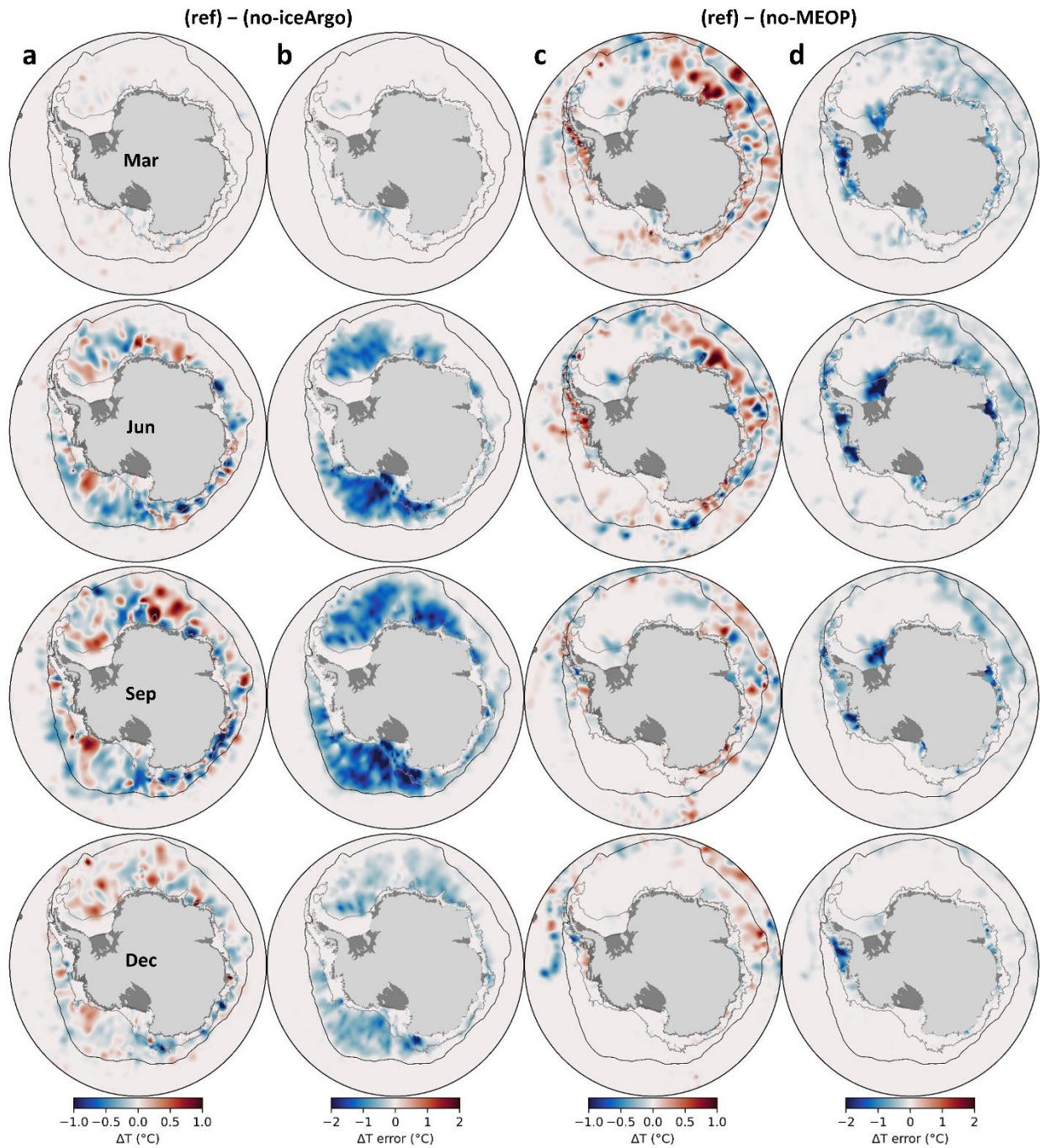
458

459

460 **Figure 3.** Zonally-averaged meridional sections. The fields displayed by row are: climatological  
 461 temperature, standard deviation of monthly temperature values ( $^{\circ}\text{C}$ ), climatological salinity, and  
 462 standard deviation of monthly salinity values (practical salinity unit), derived from (a) DIVA, (b)  
 463 WOA23, and (c) B-SOSE. Differences between DIVA and WOA23 (d), as well as DIVA and B-  
 464 SOSE (e), are also shown. White contour denotes the  $0^{\circ}\text{C}$  isotherm and 34.00 isohaline for  
 465 DIVA (solid line) and for WOA23 and B-SOSE (dashed line). A vertical dotted line corresponds  
 466 to the mean latitude of the sea ice extent in September.

467

468



469

470

471 **Figure 4.** Impact of the under-ice observations. Monthly difference between the reference  
 472 climatology and the “no-iceArgo” climatology is shown for (a) temperature and (b) temperature  
 473 interpolation error at 100 m, representing the effect of under-ice Argo data. Panels (c) and (d) are  
 474 those for “no-MEOP”, representing the effect of biologging data. The 3,000 m isobath of the  
 475 continental slope and the climatological sea ice extent in September are shown as in Figure 1.  
 476